

Differentiable SpaTiaL: Symbolic Learning and Reasoning with Geometric Temporal Logic for Manipulation Tasks

Licheng Luo¹, Kaier Liang², Cristian-Ioan Vasile², Mingyu Cai¹

Abstract—Executing complex manipulation in cluttered environments requires satisfying coupled geometric and temporal constraints. Although Spatio-Temporal Logic (SpaTiaL) offers a principled specification framework, its use in gradient-based optimization is limited by non-differentiable geometric operations. Existing differentiable temporal logics focus on the robot’s internal state and neglect interactive object–environment relations, while spatial logic approaches that capture such interactions rely on discrete geometry engines that break the computational graph and preclude exact gradient propagation. To overcome this limitation, we propose *Differentiable SpaTiaL*, a fully tensorized toolbox that constructs smooth, autograd-compatible geometric primitives directly over polygonal sets. To the best of our knowledge, this is the first end-to-end differentiable symbolic spatio-temporal logic toolbox. By analytically deriving differentiable relaxations of key spatial predicates—including signed distance, intersection, containment, and directional relations—we enable an end-to-end differentiable mapping from high-level semantic specifications to low-level geometric configurations, without invoking external discrete solvers. This fully differentiable formulation unlocks two core capabilities: (i) massively parallel trajectory optimization under rigorous spatio-temporal constraints, and (ii) direct learning of spatial logic parameters from demonstrations via backpropagation. Experimental results validate the effectiveness and scalability of the proposed framework.

I. INTRODUCTION

Robotic manipulation in human-shared and cluttered environments demands behaviors that satisfy rich, tightly coupled spatio-temporal constraints. Beyond simple collision avoidance, robots must maintain safety margins around dynamic obstacles, operate within confined workspaces, and enforce structured geometric relations over time—for example, eventually placing object A inside region B while keeping it strictly to the left of object C, or transporting an object without intersecting restricted zones throughout execution. Such requirements are inherently relational, involving multi-object interactions, spatial topology, and temporal ordering. Signal Temporal Logic (STL) [1]–[3], augmented with spatial set-theoretic semantics as in Spatio-Temporal Logic (SpaTiaL) [4], provides a rigorous and expressive formalism to encode these specifications [5]. This logical framework enables precise reasoning over time-indexed geometric predicates and supports robustness metrics that quantify satisfaction. However, despite its expressiveness, a fundamental challenge in modern robotics is to integrate such high-level logical structure directly into gradient-based trajectory optimization and deep learning pipelines, thereby enabling

end-to-end synthesis and inference of complex behaviors [6]–[11]. The key limitation lies in the incompatibility between geometric spatial reasoning and gradient-based backpropagation. Spatial predicates are typically evaluated through discrete collision detection, combinatorial topology checks, or non-smooth distance queries, all of which break differentiability. Recent advances in differentiable temporal logic, such as STL_{CG} [12], [13], have successfully reformulated temporal operators as smooth computation graphs, enabling gradient propagation through logical structure. Yet, these approaches operate primarily over system state variables and do not natively capture multi-dimensional geometric extents, object–object interactions, continuous object boundaries, or spatial topological relations. As a result, the expressive power of spatio-temporal logic remains largely disconnected from modern differentiable optimization and learning frameworks.

Conversely, existing spatial logic frameworks that evaluate geometric relations rely heavily on discrete collision checkers or classical geometry engines (e.g., Shapely [14], FCL [15]). These engines utilize discrete algorithmic branches and non-differentiable boolean operations. Consequently, the evaluation of spatial predicates fractures the computational graph, precluding gradients from flowing backward from the logical robustness loss to the physical robot states. To bypass this, prior works are often forced to employ grid-based spatial discretizations or heuristic gradient maps, which suffer drastically from the curse of dimensionality and remain computationally intractable for high-degree-of-freedom manipulation tasks [16], [17].

To overcome this limitation, we introduce *Differentiable SpaTiaL*. We mathematically formulate differentiable approximations of the Separating Axis Theorem (SAT) [17] and soft boundary representations for convex polygonal sets, in the spirit of differentiable geometric computation [18]–[22]. By natively defining core spatial predicates—such as distance, signed penetration, overlap—as fully differentiable operations, *Differentiable SpaTiaL* establishes an unbroken computational graph. This circumvents the discrete bottlenecks of traditional collision checkers, allowing the spatial robustness signal to be differentiated analytically with respect to the continuous poses and geometries of the physical objects, as illustrated in Fig. 1.

To highlight our core positioning, Table I contrasts our framework with existing approaches. While differentiable temporal-logic toolboxes such as STL_{CG} [12] excel at temporal reasoning and support gradient-based optimization over temporal specifications on real-valued signals, they do not natively provide object-centric geometric predicates.

¹UC Riverside {lichengl, mingyuc}@ucr.edu. ²Lehigh University {kal221, cvasile}@lehigh.edu. Code Available: <https://github.com/plenllune/DiffSpaTiaL>

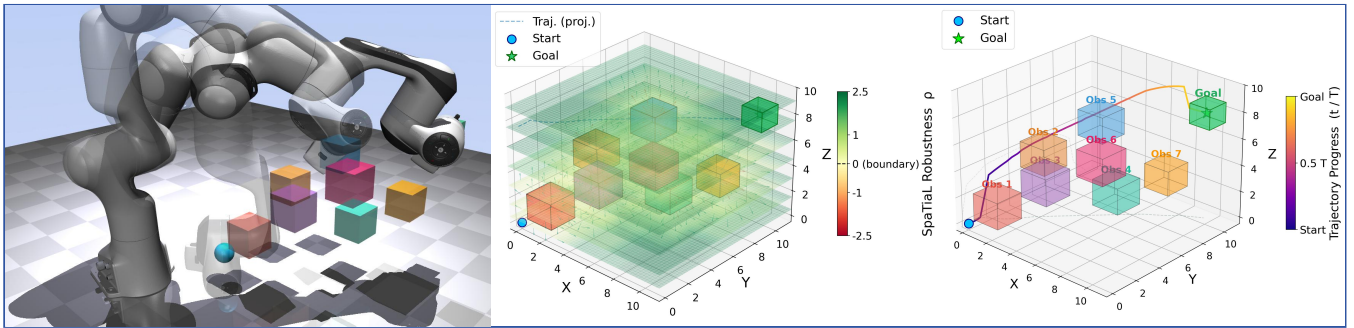


Fig. 1: Overview of *Differentiable SpaTiaL*. Our framework replaces discrete geometry engines with a fully tensorized architecture, enabling end-to-end trajectory optimization under formal specifications.

Differentiable geometry engines such as DiffCol [21] focus on geometric collision queries and derivatives rather than compositional temporal-logic semantics. To the best of our knowledge, *Differentiable SpaTiaL* is the first end-to-end differentiable spatio-temporal logic toolbox designed for gradient-based continuous optimization.

TABLE I: Feature comparison of our toolbox against existing formal logic and geometric frameworks.

Framework / Toolbox	Temporal	Spatial	Differentiable	Batch-native tensorized
Diff-TL (e.g., STLGC [12], [13])	✓	×	✓	✓
SpaTiaL [4]	✓	✓	×	×
Diff. Collision (e.g., DiffCol [21])	×	✓	✓	×
Diff-SpaTiaL (Ours)	✓	✓	✓	✓

By unifying geometric reasoning with automatic differentiation, our framework provides a scalable mathematical foundation for spatio-temporal logic in modern learning pipelines. The main contributions of this paper are:

- We develop *Differentiable SpaTiaL*, to the best of our knowledge the first fully tensorized toolbox for geometric spatial predicates based on smooth SAT and boundary-sampled SDF, enabling dense gradients while avoiding discrete grid-based or iterative search bottlenecks.
- We present a unified gradient-based framework that integrates scalable multi-object spatio-temporal constraints into a single optimization objective, enabling formal specifications to be incorporated into GPU-based optimization workflows.
- We introduce a principled approach for inferring and refining SpaTiaL specifications by optimizing continuous geometric parameters directly from human demonstrations, achieved through end-to-end backpropagation over spatial robustness metrics.

II. RELATED WORK

A. Differentiable Temporal Logic and Robustness

STL is widely used to specify operational requirements in continuous control [1]–[3], [5]. Building on this, extensive research has leveraged STL for trajectory optimization and generation, employing techniques ranging from Mixed-Integer Linear Programming (MILP) [23] and probabilistic approaches under uncertainty [24], to continuous smoothing [25] and Recurrent Neural Networks (RNNs) [26]. A pivotal development in scaling these methods is differentiable robustness computation [12], which approximates non-

smooth min / max operators to allow analytic gradient propagation through temporal operators. While these frameworks successfully tensorize the temporal dimension, extending them to natively handle complex geometric sets remains an open challenge. They often assume atomic predicates are pre-defined, differentiable scalar functions of low-dimensional states, which complicates the direct evaluation of multi-dimensional physical shapes (e.g., polygons).

B. Differentiable Collision Detection and Geometry

To integrate geometric reasoning into gradient-based pipelines, recent advancements in differentiable physics compute gradients through collision detection algorithms (e.g., GJK/EPA-style convex proximity pipelines [16], [17]) via randomized smoothing, differentiable simulation, or implicit differentiation [18]–[22]. Although these methods maintain exact geometric witness points, their iterative nature introduces challenges for vectorization. This computational overhead can be a limiting factor for batch-heavy, long-horizon trajectory optimization [10], [11], [15]. Similarly, while the foundational SpaTiaL framework [4] successfully pioneers spatio-temporal logic for task planning, its spatial predicates traditionally rely on these discrete geometric evaluations. To overcome this bottleneck, *Differentiable SpaTiaL* relaxes the need for exact discrete iterations. By formulating continuous approximations of the SAT and soft boundary representations, the proposed architecture natively supports massive GPU parallelism, facilitating the computational efficiency required for deep learning pipelines.

C. Learning and Inference of Logical Specifications

To complement opaque neural policies, a parallel line of research infers interpretable logical specifications from demonstrations [27]–[30]. These methods optimize discrete formula structures and continuous parameters using mixed-integer programming [31] or neural-symbolic networks [32], typically guided by continuous robustness [2], [3], [12]. However, extending these frameworks to complex physical environments reveals a critical bottleneck: exact geometric evaluations incur prohibitive computational costs in discrete optimization, and their non-differentiable nature severs the computational graph in gradient-based learning. Consequently, prior methods are fundamentally restricted to simplified, non-geometric state predicates. By establishing a

natively differentiable geometric foundation, our framework overcomes this barrier. It tensorizes spatial set reasoning, enabling continuous geometric parameters—such as target boundaries and safety margins—to be directly inferred via backpropagation through spatial robustness.

III. PROBLEM FORMULATION

This section introduces the STL [1] and SpaTiaL [4] preliminaries used in this work, and then states our differentiable robustness formulation problem.

A. Signal Temporal Logic

We consider a discrete-time finite-horizon trajectory $\xi = \{s_0, s_1, \dots, s_T\}$, where each state $s_t \in \mathbb{R}^n$ represents the geometric configurations of the robotic system and all objects in the workspace at time step t . STL formulas ϕ specify temporal properties over the trajectory ξ . An atomic predicate is defined as $\mu := a^\top s_t \geq b$ with $a \in \mathbb{R}^n$ and $b \in \mathbb{R}$. The grammar of STL is:

$$\phi ::= \mu \mid \neg\phi \mid \phi_1 \wedge \phi_2 \mid \phi_1 \vee \phi_2 \quad (1)$$

where $0 \leq k_1 \leq k_2$ are integer time bounds representing the evaluation window $[t + k_1, t + k_2]$. The operators F, G , and U denote *eventually*, *always*, and *until*, respectively.

Quantitative robustness $\rho(\xi, \phi, t)$ measures the degree of satisfaction: $\rho(\xi, \phi, t) > 0$ if ξ satisfies ϕ at time t , and $\rho(\xi, \phi, t) < 0$ otherwise. This metric enables the transformation of logical requirements into continuous optimization objectives [3]. For a trajectory ξ , the exact robustness is defined recursively:

$$\begin{aligned} \rho(\xi, \mu, t) &= a^\top s_t - b & (2) \\ \rho(\xi, \neg\phi, t) &= -\rho(\xi, \phi, t), \\ \rho(\xi, \phi_1 \wedge \phi_2, t) &= \min(\rho(\xi, \phi_1, t), \rho(\xi, \phi_2, t)), \\ \rho(\xi, G_{[k_1, k_2]}\phi, t) &= \min_{t' \in [t+k_1, t+k_2]} \rho(\xi, \phi, t'), \\ \rho(\xi, F_{[k_1, k_2]}\phi, t) &= \max_{t' \in [t+k_1, t+k_2]} \rho(\xi, \phi, t'). \end{aligned}$$

By convention, the system satisfies the specification if the initial robustness is positive, i.e., $\rho(\xi, \phi, 0) > 0$.

B. SpaTiaL: Geometry-based Spatial Predicates

We adopt the SpaTiaL fragment [4] over compact convex sets $\mathcal{P}_i \subset \mathbb{R}^n$ ($n \in \{2, 3\}$), whose vertices and headings define the scene state s_t . Its spatial atoms are derived from signed distances and axis-aligned projections, yielding quantitative semantics compatible with STL monitoring.

Definition 1 (SpaTiaL Atomic Predicates [4]). *For distinct objects i, j and constants $\varepsilon, \varepsilon_c, \varepsilon_f, \delta_{ov}, \delta_{in}, \kappa > 0$, let $\text{dist}(\mathcal{P}_i, \mathcal{P}_j) = \min_{u \in \mathcal{P}_i, v \in \mathcal{P}_j} \|u - v\|$ be the minimum Euclidean distance. Let $\text{pen}(\mathcal{P}_i, \mathcal{P}_j)$ denote the penetration depth. We define the signed clearance as $\text{clr}_{ij} = \text{dist}(\mathcal{P}_i, \mathcal{P}_j)$ if $\mathcal{P}_i \cap \mathcal{P}_j = \emptyset$, and $\text{clr}_{ij} = -\text{pen}(\mathcal{P}_i, \mathcal{P}_j)$ otherwise. Let $\max_x(\mathcal{P}_i) = \max_{u \in \mathcal{P}_i} u_x$ and $\min_x(\mathcal{P}_i) = \min_{u \in \mathcal{P}_i} u_x$ denote the bounding coordinates of \mathcal{P}_i along the x -axis (analogously for y and z axes). The geometric atomic predicates are defined as follows:*

- $\text{closeTo}_\varepsilon(i, j) : \text{dist}(\mathcal{P}_i, \mathcal{P}_j) \leq \varepsilon_c$
- $\text{farFrom}_\varepsilon(i, j) : \text{dist}(\mathcal{P}_i, \mathcal{P}_j) \geq \varepsilon_f$
- $\text{Touch}(i, j) : |\text{clr}_{ij}| \leq \varepsilon$
- $\text{ovlp}(i, j) : \text{clr}_{ij} < -\delta_{ov}$
- $\text{partOvlp}(i, j) : \text{ovlp}(i, j) \wedge \neg \text{enclIn}(i, j) \wedge \neg \text{enclIn}(j, i)$
- $\text{enclIn}(i, j) : \mathcal{P}_i \subset (\mathcal{P}_j \ominus \mathcal{B}_{\delta_{in}})$
- $\text{LeftOf}(i, j) : \max_x(\mathcal{P}_i) + \kappa \leq \min_x(\mathcal{P}_j)$
- $\text{RightOf}(i, j) : \max_x(\mathcal{P}_j) + \kappa \leq \min_x(\mathcal{P}_i)$
- $\text{Behind}(i, j) : \max_y(\mathcal{P}_i) + \kappa \leq \min_y(\mathcal{P}_j)$
- $\text{InFrontOf}(i, j) : \max_y(\mathcal{P}_j) + \kappa \leq \min_y(\mathcal{P}_i)$
- $\text{Below}(i, j) : \max_z(\mathcal{P}_i) + \kappa \leq \min_z(\mathcal{P}_j)$
- $\text{Above}(i, j) : \max_z(\mathcal{P}_j) + \kappa \leq \min_z(\mathcal{P}_i)$
- $\text{Between}_{\text{px}}(a, b, c) : \max_x(\mathcal{P}_a) + \kappa \leq \min_x(\mathcal{P}_b) \wedge \max_x(\mathcal{P}_b) + \kappa \leq \min_x(\mathcal{P}_c)$
- $\text{Between}_{\text{py}}(a, b, c) : \max_y(\mathcal{P}_a) + \kappa \leq \min_y(\mathcal{P}_b) \wedge \max_y(\mathcal{P}_b) + \kappa \leq \min_y(\mathcal{P}_c)$
- $\text{oriented}(i, j; \kappa) : \text{ecd}(u_i, u_j) \leq \kappa$

where \ominus denotes set erosion (Pontryagin difference), i.e., $\mathcal{A} \ominus \mathcal{B} = \{x \mid x + \mathcal{B} \subseteq \mathcal{A}\}$, $\mathcal{B}_{\delta_{in}}$ is a ball of radius δ_{in} , u_i is the unit heading of object i , and $\text{ecd}(u_i, u_j) = \frac{1}{2} \|u_i - u_j\|_2^2$.

Definition 2 (Quantitative Semantics). *Let $\rho(s_t, \cdot)$ denote the exact robustness of a geometric atomic predicate under scene state s_t . The quantitative semantics are:*

- $\rho(\text{closeTo}_\varepsilon(i, j)) = \varepsilon_c - \text{dist}(\mathcal{P}_i, \mathcal{P}_j)$
- $\rho(\text{farFrom}_\varepsilon(i, j)) = \text{dist}(\mathcal{P}_i, \mathcal{P}_j) - \varepsilon_f$
- $\rho(\text{Touch}(i, j)) = -|\text{clr}_{ij}| + \varepsilon$
- $\rho(\text{ovlp}(i, j)) = -\text{clr}_{ij} - \delta_{ov}$
- $\rho(\text{partOvlp}(i, j)) = \min(\rho(\text{ovlp}(i, j)), -\rho(\text{enclIn}(i, j)), -\rho(\text{enclIn}(j, i)))$
- $\rho(\text{enclIn}(i, j)) = -\delta_{in} - \max_{u \in \mathcal{P}_i} \text{sd}(u, \partial\mathcal{P}_j)$
- $\rho(\text{LeftOf}(i, j)) = \min_x(\mathcal{P}_j) - \max_x(\mathcal{P}_i) - \kappa$
- $\rho(\text{RightOf}(i, j)) = \min_x(\mathcal{P}_i) - \max_x(\mathcal{P}_j) - \kappa$
- $\rho(\text{Behind}(i, j)) = \min_y(\mathcal{P}_j) - \max_y(\mathcal{P}_i) - \kappa$
- $\rho(\text{InFrontOf}(i, j)) = \min_y(\mathcal{P}_i) - \max_y(\mathcal{P}_j) - \kappa$
- $\rho(\text{Below}(i, j)) = \min_z(\mathcal{P}_j) - \max_z(\mathcal{P}_i) - \kappa$
- $\rho(\text{Above}(i, j)) = \min_z(\mathcal{P}_i) - \max_z(\mathcal{P}_j) - \kappa$
- $\rho(\text{Between}_{\text{px}}(a, b, c)) = \min(\min_x(\mathcal{P}_b) - \max_x(\mathcal{P}_a) - \kappa, \min_x(\mathcal{P}_c) - \max_x(\mathcal{P}_b) - \kappa)$
- $\rho(\text{Between}_{\text{py}}(a, b, c)) = \min(\min_y(\mathcal{P}_b) - \max_y(\mathcal{P}_a) - \kappa, \min_y(\mathcal{P}_c) - \max_y(\mathcal{P}_b) - \kappa)$
- $\rho(\text{oriented}(i, j; \kappa)) = \kappa - \frac{1}{2} \|u_i - u_j\|_2^2$

where $\text{sd}(u, \partial\mathcal{P}_j)$ denotes the signed distance from point u to the boundary of \mathcal{P}_j (negative if u is strictly inside \mathcal{P}_j).

C. Differentiable Problem Formulation

Given the scene trajectory ξ , let ϕ be a spatio-temporal specification formed by composing STL temporal operators with SpaTiaL spatial predicates. The corresponding exact robustness at time 0 is denoted by $\rho(\xi, \phi, 0)$.

The central objective of this paper is to construct a differentiable surrogate robustness $\tilde{\rho}(\xi, \phi, 0)$ for SpaTiaL-based specifications, such that it remains semantically faithful to $\rho(\xi, \phi, 0)$ while enabling end-to-end gradient propagation with respect to geometric states. Specifically, we seek a

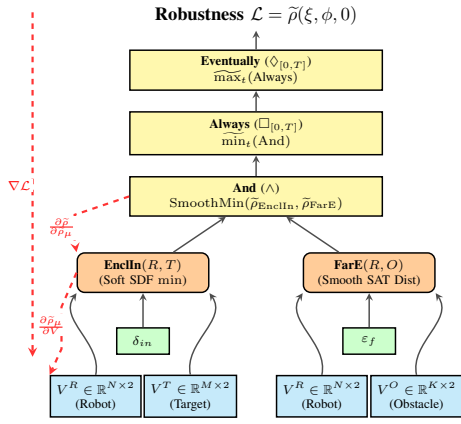


Fig. 2: Smooth spatial and temporal operators form a differentiable robustness computation graph.

formulation such that $\tilde{\rho}(\xi, \phi, 0) \approx \rho(\xi, \phi, 0)$, and $\frac{\partial \tilde{\rho}(\xi, \phi, 0)}{\partial s_t}$ exists and remains informative for all $t \in \{0, \dots, T\}$.

The difficulty is not the temporal composition itself, since STL robustness is recursively defined through min/max-type operators, but the spatial atomic robustness terms in SpaTiaL (e.g., distance, overlap, enclosure, and directional relations). In standard implementations, these spatial quantities are evaluated by discrete geometry engines with branching logic and boolean operations, which break the computational graph and make gradients undefined or uninformative.

Therefore, the problem addressed in this work is to reformulate SpaTiaL spatial semantics over polygonal objects into a fully tensorized, smooth, and autograd-compatible computation graph. Once the spatial atomic predicates become differentiable, they can be composed with smoothed temporal operators to produce an end-to-end differentiable robustness pipeline, which directly supports gradient-based trajectory optimization and specification parameter learning.

IV. METHODOLOGY

To integrate SpaTiaL into continuous optimization, the entire evaluation pipeline must be differentiable. Here, we formulate *Differentiable SpaTiaL*, a fully tensorized computational graph that analytically relaxes discrete geometric queries into smooth spatial semantics, as outlined in Fig. 2

A. Overview of Tensorized Spatial Semantics

Consider the trajectory ξ where each state s_t is represented natively as multi-dimensional tensors (e.g., vertex coordinates of bounding polygons). To optimize ξ with respect to a high-level spatio-temporal formula ϕ via gradient descent, we define a loss function $\mathcal{L}(\tilde{\rho}(\xi, \phi, 0))$ over the quantitative smoothed logical robustness $\tilde{\rho}$, and we must compute the analytic gradient $\nabla_{\xi} \mathcal{L}$.

Applying the chain rule, the gradient flow to the geometric state at time t is decomposed as:

$$\frac{\partial \mathcal{L}}{\partial s_t} = \frac{\partial \mathcal{L}}{\partial \tilde{\rho}} \sum_k \left(\frac{\partial \tilde{\rho}}{\partial \tilde{\rho}(\mu_k)} \frac{\partial \tilde{\rho}(\mu_k)}{\partial s_t} \right), \quad (3)$$

where $\tilde{\rho}(\mu_k)$ denotes the smoothed robustness of the k -th spatial atomic predicate (e.g., distance, overlap) evaluated at time t . Existing differentiable temporal logics [12] provide

the temporal gradient mapping $\frac{\partial \tilde{\rho}}{\partial \tilde{\rho}(\mu_k)}$ by smoothing operators like *Always* and *Eventually*. However, standard geometry engines (e.g., Shapely) render the spatial gradient $\frac{\partial \tilde{\rho}(\mu_k)}{\partial s_t}$ undefined or zero almost everywhere due to discrete Boolean operations.

Differentiable SpaTiaL bridges this gap by mathematically formulating $\frac{\partial \tilde{\rho}(\mu_k)}{\partial s_t}$ natively in tensor space. We circumvent non-differentiable bottlenecks by relaxing exact geometric queries using the LogSumExp (LSE) function as a smooth maximum approximator:

$$\widetilde{\max}_{\tau}(\mathbf{x}) = \tau \log \sum_{i=1}^N \exp(x_i/\tau), \quad (4)$$

$$\widetilde{\min}_{\tau}(\mathbf{x}) = -\widetilde{\max}_{\tau}(-\mathbf{x}), \quad (5)$$

where $\tau > 0$ controls the smoothness temperature. As $\tau \rightarrow 0$, the function approaches the exact max/min operators, while $\tau > 0$ ensures a smooth, non-zero gradient landscape across the entire spatial domain.

B. Differentiable Penetration via Smooth SAT

Standard penetration depth algorithms (e.g., EPA) involve discrete iterative searches over simplices, which fracture the computational graph. Instead, we derive a smooth, fully tensorized variant of the Separating Axis Theorem (SAT) suitable for convex polygonal sets, as illustrated in Fig. 3.

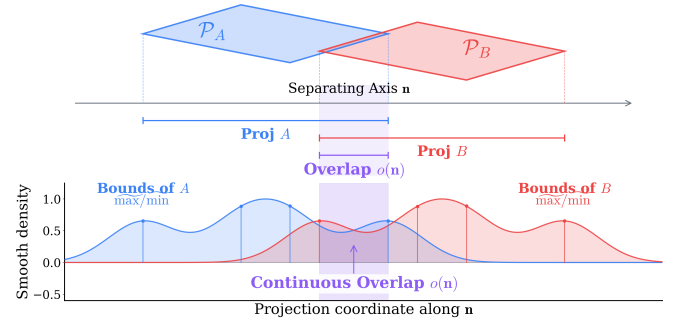


Fig. 3: Differentiable penetration depth via Smooth SAT. Exact discrete overlap is relaxed into a smooth, differentiable repulsion field.

Let \mathcal{P}_A and \mathcal{P}_B be two convex polygons parameterized by their counter-clockwise vertex tensors $\mathbf{V}^A \in \mathbb{R}^{N_A \times d}$ and $\mathbf{V}^B \in \mathbb{R}^{N_B \times d}$. Let \mathcal{N} be the combined set of all inward unit edge normals from both polygons. For a specific projection axis $\mathbf{n} \in \mathcal{N}$, the projection of polygon \mathcal{P}_A yields a continuous range $[\min(\mathbf{V}^A \mathbf{n}), \max(\mathbf{V}^A \mathbf{n})]$. Using our smooth operators, the upper and lower projection bounds are defined as $P_{\max}^A = \widetilde{\max}_{\tau}(\mathbf{V}^A \mathbf{n})$ and $P_{\min}^A = \widetilde{\min}_{\tau}(\mathbf{V}^A \mathbf{n})$.

The overlapping margin on the axis \mathbf{n} is computed as:

$$o(\mathbf{n}) = \widetilde{\min}_{\tau}(P_{\max}^A, P_{\max}^B) - \widetilde{\max}_{\tau}(P_{\min}^A, P_{\min}^B). \quad (6)$$

The differentiable penetration depth across all separating axes is then formulated by taking the smooth minimum of the overlaps:

$$pen(\mathcal{P}_A, \mathcal{P}_B) = \text{ReLU}\left(\widetilde{\min}_{\tau}(\min_{\mathbf{n} \in \mathcal{N}}(o(\mathbf{n})))\right). \quad (7)$$

This formulation yields $pen > 0$ when the polygons intersect, generating a smooth repulsion gradient analytically derived from dense matrix multiplications, entirely avoiding discrete branching.

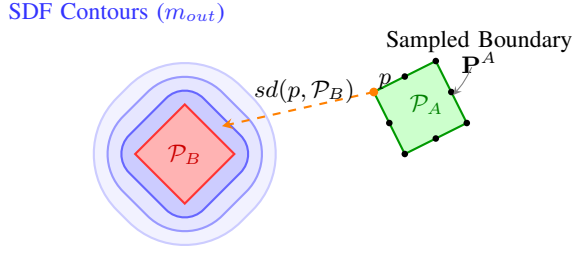


Fig. 4: Differentiable Signed Distance Field (SDF) via boundary sampling. Soft aggregation ensures informative gradients in both colliding and non-colliding states.

C. Smooth Approximations of Geometric Distances

While the SAT penetration depth handles overlapping states, evaluating strictly separated states requires a differentiable distance metric. As shown in Fig. 4, we approximate the exact boundary-to-boundary shortest path using soft boundary sampling and smooth half-space intersections. For brevity, we write $d(p, \mathcal{P}) := m_{out}(p)$ for the smooth unsigned point-to-polygon distance, use $\text{dist}(\mathcal{P}_A, \mathcal{P}_B)$ for polygon-to-polygon distance, and use sd generically for signed-distance quantities; the intended meaning is disambiguated by the argument types.

We sample a set of points \mathbf{P}^A uniformly along the perimeter of \mathcal{P}_A . For any sampled point $p \in \mathbf{P}^A$, its spatial relationship to polygon \mathcal{P}_B is evaluated via half-space constraints. Let e_i^B denote the i -th edge of \mathcal{P}_B , defined by a vertex $v_i^B \in e_i^B$ and an inward unit normal \mathbf{n}_i^B . We let $s_i = (p - v_i^B) \cdot \mathbf{n}_i^B$ denote the signed distance from p to the i -th edge of \mathcal{P}_B . The internal margin is given by $m_{in}(p) = \min_{\tau}(\{s_i\}_{i=1}^{N_B})$. To capture the external distance, we compute the smooth point-to-segment distance $d_{seg}(p, e_i^B)$ for all edges e_i^B , yielding the external margin $m_{out}(p) = \widetilde{\min}_{\tau}(\{d_{seg}\})$. The smooth signed distance for a single point p to polygon \mathcal{P}_B is smoothly blended using a sigmoid weighting function $w(p) = \sigma(k \cdot m_{in}(p))$, where $\sigma(x) = 1/(1 + \exp(-x))$ and k is a scaling constant:

$$\text{sd}(p, \mathcal{P}_B) = (1 - w(p)) \cdot m_{out}(p) - w(p) \cdot m_{in}(p). \quad (8)$$

A negative value strictly indicates that p is enclosed within \mathcal{P}_B . The symmetric unsigned distance between the two polygons is aggregated over all boundary samples:

$$\text{dist}(\mathcal{P}_A, \mathcal{P}_B) \approx \widetilde{\min}_{\tau} \left(\widetilde{\min}_{p \in \mathbf{P}^A} d(p, \mathcal{P}_B), \widetilde{\min}_{p \in \mathbf{P}^B} d(p, \mathcal{P}_A) \right) \quad (9)$$

By unifying the smooth SAT penetration (Eq. 7) and the soft boundary distance (Eq. 9), we define a universally differentiable signed distance $\text{sd}(\mathcal{P}_A, \mathcal{P}_B)$. This metric serves as the quantitative smoothed robustness value q for distance-based spatial predicates (e.g., $\text{closeTo}_{\varepsilon}$, $\text{farFrom}_{\varepsilon}$).

D. Compositional Spatial Predicates

Leveraging the tensorized spatial primitives, higher-level topological and directional relations in the SpaTialL grammar are synthesized purely through differentiable algebraic operations, as depicted in Fig. 5.

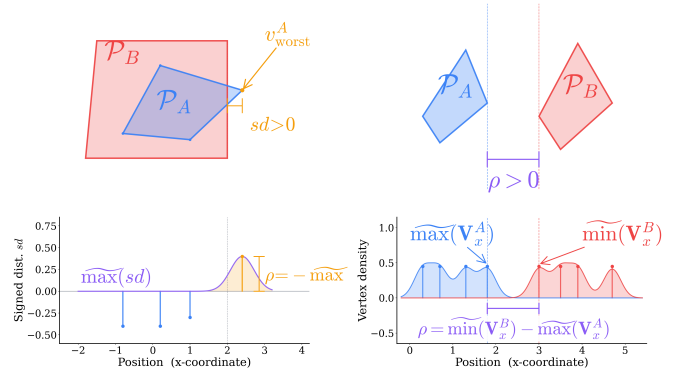


Fig. 5: Geometric interpretation of compositional predicates (left: EncIn, right: leftOf). Spatial relations are resolved as differentiable algebraic operations over vertex tensors.

1) *Enclosure and Containment*: The predicate $\text{encIn}(\mathcal{P}_A, \mathcal{P}_B)$ requires all parts of \mathcal{P}_A to reside strictly within \mathcal{P}_B . Utilizing the point-to-polygon signed distance, the smooth atomic robustness q is computed by extracting the least enclosed (most outward) point of \mathcal{P}_A :

$$\tilde{\rho}(\text{encIn}(A, B)) = -\delta_{in} - \widetilde{\max}_{\tau}(\{sd(v_i^A, \mathcal{P}_B) \mid v_i^A \in \mathbf{V}^A\}). \quad (10)$$

A robustness $\tilde{\rho} \geq 0$ indicates strict geometric containment.

2) *Directional Projections*: Predicates evaluating relative poses, such as LeftOf or Above, are formulated by projecting the geometric centroids or bounding vertices onto the global coordinate axes. Let c_A and c_B be the differentiable centroids of the polygons. The smooth atomic robustness for LeftOf is straightforwardly defined via smooth coordinate comparisons:

$$\tilde{\rho}(\text{LeftOf}(A, B)) = \widetilde{\min}_{\tau}(\mathbf{V}_x^B) - \widetilde{\max}_{\tau}(\mathbf{V}_x^A) - \kappa, \quad (11)$$

where \mathbf{V}_x denotes the x-coordinate tensor of the vertices.

3) *Relative Bearing*: For orientation-dependent tasks, the predicate evaluates the bearing from object A to object B . The relative angle is obtained via the differentiable arc-tangent function applied to the centroid displacements: $\tilde{\rho}(\text{BearingTo}(A, B, \theta_{ref})) = \kappa - \|\text{atan2}(c_B^y - c_A^y, c_B^x - c_A^x) - \theta_{ref}\|_2^2$, where κ is the tolerance threshold. By executing these compositional predicates as vectorized tensor operations, the framework enables complex spatial conditions to be efficiently evaluated and differentiated across massive batches of state trajectories.

The constructions above establish differentiable implementations of representative compositional predicates. Beyond differentiability, however, we also require a basic semantic guarantee: the smooth relaxation should not artificially overestimate predicate satisfaction. In particular, for safety-critical optimization, it is desirable that positive smoothed robustness implies positive exact robustness (i.e., a conservative approximation). We next show that this property follows from standard LogSumExp (LSE) bounds for the core predicate primitives used in our framework.

Lemma 1. For any vector $\mathbf{x} \in \mathbb{R}^N$ and temperature $\tau > 0$:

$$\max(\mathbf{x}) \leq \widetilde{\max}(\mathbf{x}) \leq \max(\mathbf{x}) + \tau \log N, \quad (12)$$

$$\min(\mathbf{x}) - \tau \log N \leq \widetilde{\min}(\mathbf{x}) \leq \min(\mathbf{x}). \quad (13)$$

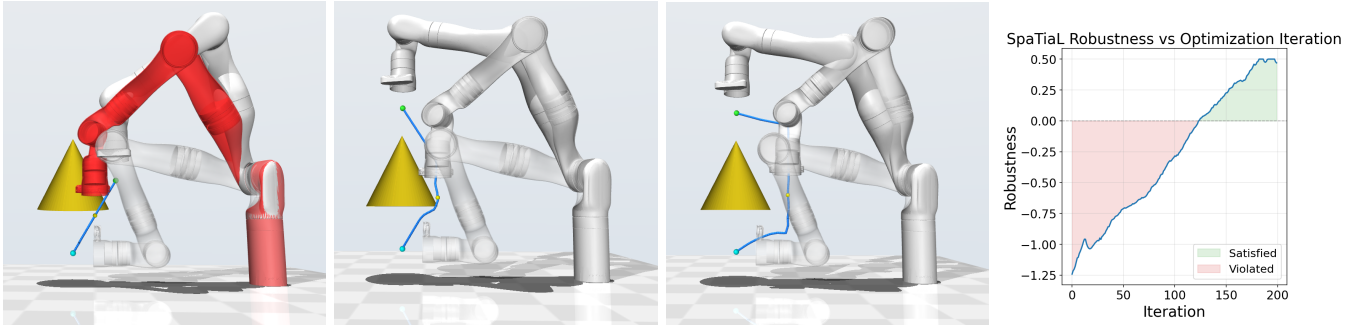


Fig. 6: Qualitative spatio-temporal trajectory optimization using differentiable spatial semantics. From left to right: initial trajectory (violates), iteration 30, final trajectory (satisfies), and robustness analysis.

Here $\widetilde{\min}$ and $\widetilde{\max}$ denote the LSE-based smooth relaxations of \min and \max , respectively. By Lemma 1, we directly obtain $\widetilde{\min}(\mathbf{x}) \leq \min(\mathbf{x})$, $\widetilde{\max}(\mathbf{x}) \geq \max(\mathbf{x})$.

Theorem 1. *We assume throughout that the specification is in positive normal form, without significant loss of generality in our setting. For convex polygons with exact vertex representations and $\tau > 0$:*

- (i) Any *spatial predicate* whose robustness is a single-level \min or negated $\widetilde{\max}$ over exact scalar quantities (directional predicates) satisfies $\widetilde{\rho}(\phi) \leq \rho_{\text{exact}}(\phi)$.
- (ii) For predicates involving boundary sampling or nested smooth operators (farFrom $_{\varepsilon}$, closeTo $_{\varepsilon}$, enclIn, ovlp, Touch), $\widetilde{\rho}(\phi) \leq \rho_{\text{exact}}(\phi) + \delta$, where $\delta = O(\tau \log N + h)$ depends on the LSE temperature τ , polygon complexity N , and sampling spacing h . Both error sources vanish as $\tau \rightarrow 0$ and $h \rightarrow 0$.
- (iii) ORIENTED is exact: $\widetilde{\rho} = \rho_{\text{exact}}$.

Proof. *Case (i):* Directional predicates are sums of extremal coordinate terms with \min / \max replaced by $\widetilde{\min} / \widetilde{\max}$. By Lemma 1, each smooth extremum is conservative, so $\widetilde{\rho}(\phi) \leq \rho_{\text{exact}}(\phi)$ and $\widetilde{\rho}(\phi) > 0 \implies \rho_{\text{exact}}(\phi) > 0$.

Case (ii): For enclIn, the outer term satisfies $-\widetilde{\max}_i g_i \leq -\max_i g_i$, but each $g_i = \text{sd}(v_i^A, \mathcal{P}_B)$ is itself smoothed, contributing $O(\tau \log N_B)$ error. For farFrom $_{\varepsilon}$, closeTo $_{\varepsilon}$, ovlp, Touch, boundary sampling contributes $O(h)$ and nested smooth aggregation contributes $O(\tau \sum_{k=1}^L \log N_k)$. Hence $\widetilde{\rho}(\phi) \leq \rho_{\text{exact}}(\phi) + \delta$ with $\delta \leq Ch + \tau \sum_{k=1}^L \log N_k$ and $h = 0$ for enclIn. Thus $\widetilde{\rho}(\phi) - \delta > 0 \implies \rho_{\text{exact}}(\phi) > 0$, and $\delta \rightarrow 0$ as $\tau, h \rightarrow 0$.

Case (iii): ORIENTED is exact, so $\widetilde{\rho}(\phi) = \rho_{\text{exact}}(\phi)$. \square

This result establishes a conservative smoothing property. For single-level predicates (Cases *i*, *iii*), the smooth robustness does not overestimate the exact value; in particular, Case *i* is conservative and Case *iii* is exact, thereby precluding false positives. For Case *ii*, a bounded overestimation δ may arise, but it vanishes as $\tau, h \rightarrow 0$, preserving a safety-oriented semantic bias in practice.

E. Robotic Applications

By unifying the temporal and spatial domains into a single end-to-end differentiable computation graph, our framework unlocks gradient-based methods for two primary robotic applications:

1) *Trajectory Optimization:* Under our framework, the robustness becomes a differentiable functional of the trajectory $\widetilde{\rho}(\xi, \phi, 0) = F_{\phi}(s_0, \dots, s_T)$, where F_{ϕ} is a smooth computation graph induced by the logical structure of ϕ . Trajectory synthesis can therefore be formulated as $\max_{\xi} \widetilde{\rho}(\xi, \phi, 0)$ subject to optional system dynamics $s_{t+1} = f(s_t, u_t)$, $u_t \in \mathcal{U}$, and state or control constraints. The gradients of $\widetilde{\rho}(\xi, \phi, 0)$ can be computed using automatic differentiation: $\nabla_{\xi} \widetilde{\rho}(\xi, \phi, 0) = \left[\frac{\partial \widetilde{\rho}}{\partial s_0}, \frac{\partial \widetilde{\rho}}{\partial s_1}, \dots, \frac{\partial \widetilde{\rho}}{\partial s_T} \right]$. The trajectory can then be iteratively updated using gradient-based optimization, $\xi^{k+1} = \xi^k + \alpha_k \nabla_{\xi} \widetilde{\rho}(\xi^k, \phi, 0)$, where α_k is the step size. This formulation transforms logical satisfaction into a continuous optimization problem, where robustness gradients provide dense feedback that progressively resolves spatial violations and steers trajectories toward specification satisfaction without combinatorial search, as shown in Fig. 6.

2) *Specification Inference:* Conversely, given a dataset of expert demonstrations $\mathcal{D} = \{\xi_i\}_{i=1}^N$, the framework also enables *learning the parameters of the specification*. Let the spatial-temporal specification be parameterized by $\theta \in \Theta \subset \mathbb{R}^p$, $\phi = \phi_{\theta}$, where θ represents continuous geometric quantities such as safety margins, object spatial relations. A spatial predicate can be written as $\mu_{\theta}(x) = g(x; \theta) \geq 0$. Using the differentiable robustness functional, each trajectory induces $\rho_i(\theta) = \widetilde{\rho}(\xi_i, \phi_{\theta}, 0)$, which measures the satisfaction margin of ξ_i . The parameters are learned by minimizing a robustness-based loss $\min_{\theta \in \Theta} \mathcal{L}(\theta) = \frac{1}{N} \sum_{i=1}^N \ell(\rho_i(\theta))$. Since spatial predicates and logical operators are implemented as smooth tensor operations, $\rho_i(\theta)$ is differentiable and gradients can be obtained via automatic differentiation: $\nabla_{\theta} \mathcal{L}(\theta) = \frac{1}{N} \sum_{i=1}^N \ell'(\rho_i(\theta)) \nabla_{\theta} \widetilde{\rho}(\xi_i, \phi_{\theta}, 0)$. This enables end-to-end inference of geometric specification parameters directly from demonstrations.

V. EXPERIMENTS

We evaluate *Differentiable SpaTial* on two capabilities enabled by our tensorized spatial semantics: (i) gradient-based spatio-temporal trajectory optimization in cluttered scenes, and (ii) learning continuous spatial specification parameters from demonstrations. All experiments are implemented in PyTorch and executed on a single NVIDIA RTX 4090 GPU. Unless stated otherwise, we use $\tau = 10^{-2}$ for smooth \min / \max (LogSumExp), boundary sampling density $S =$

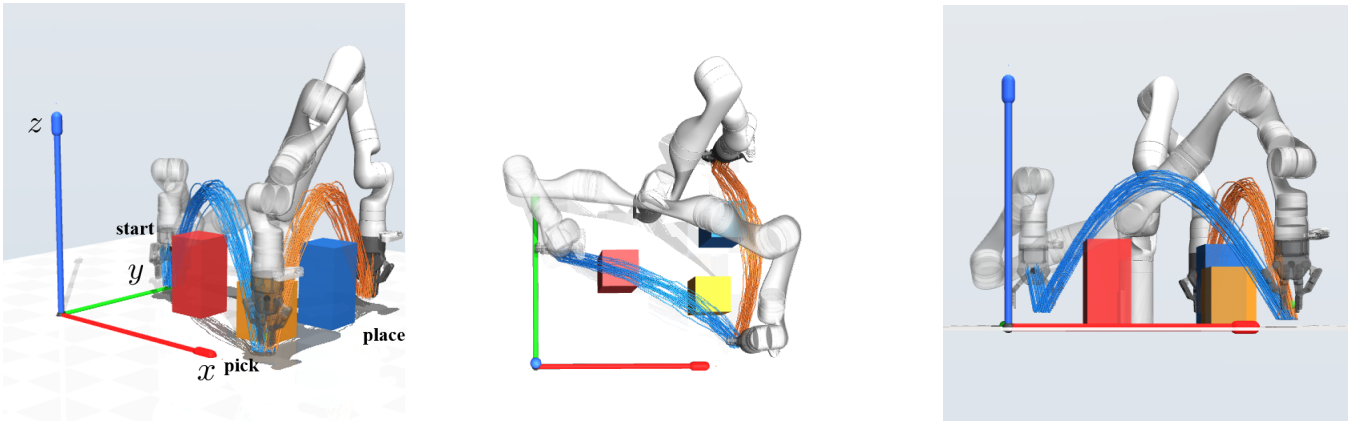


Fig. 7: Learning spatial specification parameters from demonstrations via robustness backpropagation. From left to right: oblique, xy, and xz views.

16 points per edge, and Minkowski support sampling with $\text{NUM_DIR} = 128$ directions.

A. Task I: Spatio-Temporal Trajectory Optimization

a) Specification: We consider a planar manipulation proxy where the end-effector (or object footprint) must remain safely separated from obstacles while eventually reaching a goal region. A representative specification is $\phi_{\text{opt}} = G(\text{farFrom}_{\epsilon}(\text{EE}, \text{Obs})) \wedge F_{[0, T]}(\text{enclIn}(\text{EE}, \text{Goal}))$, where EE denotes the robot end-effector, Obs denotes the obstacles, and Goal is the target region.

b) Optimization objective: We maximize the smoothed robustness by minimizing a hinge loss with a small trajectory smoothness regularizer:

$$\mathcal{L}(\xi) = \max(0, \eta - \tilde{\rho}(\xi, \phi_{\text{opt}}, 0)) + \lambda \mathcal{R}(\xi), \quad (14)$$

where $\eta > 0$ is the desired robustness margin and $\mathcal{R}(\xi)$ encourages smooth motion in pose space.

c) Qualitative results: Fig. 6 shows typical optimization behavior. Starting from an infeasible initialization (e.g., obstacle penetration and/or failure to achieve enclosure), gradients backpropagated through smooth SAT and boundary-sampled signed distance progressively push the trajectory toward feasibility. In practice, we observe three consistent phases: (i) a rapid “collision resolution” stage where repulsive gradients remove overlaps, (ii) a “constraint shaping” stage where the path adjusts to satisfy *Always*-type clearance, and (iii) a “task completion” stage where the *Eventually* clause becomes positive and the robustness margin increases.

d) Convergence: The rightmost panel of Fig. 6 plots robustness (and/or loss) over iterations. We typically observe a monotonic increase in robustness after a short warm-up period, indicating that the spatial gradients remain informative in both separated and intersecting regimes. Compared to optimization driven by sparse collision signals, our smooth predicates yield dense gradients that reduce stagnation near contact configurations.

B. Task II: Learning Spatial Specification Parameters

We show that spatial specifications can be automatically extracted from demonstrations by leveraging the differentiability of our robustness measure.

TABLE II: Discovered spatio-temporal specification with learned margins; phase 1 ($I_1 = [0, 59]$) and phase 2 ($I_2 = [60, 118]$). All predicates are of the form (arm, O_k) .

Start→Pick			Pick→Place		
Obs	Formula	ϵ	Obs	Formula	ϵ
O_1	$F_{I_1}(\text{RightOf})$	4.25	O_1	$G_{I_2}(\text{RightOf})$	3.31
	$F_{I_1}(\text{Behind})$	1.87		$F_{I_2}(\text{InFrontOf})$	3.77
O_2	$F_{I_1}(\text{LeftOf})$	5.25	O_2	$F_{I_2}(\text{InFrontOf})$	4.73
	$F_{I_1}(\text{Above})$	2.55		$F_{I_2}(\text{Above})$	2.52
O_3	$F_{I_1}(\text{LeftOf})$	5.83	O_3	$F_{I_2}(\text{Behind})$	3.66
	$F_{I_1}(\text{Behind})$	3.76		$F_{I_2}(\text{Above})$	1.57

Given 30 demonstration trajectories from a 3D pick-and-place task with three box obstacles in a $[0, 10]^3$ workspace (Fig. 7), where the robot base is at $(5, 7, 0)$, we proceed in two steps. **(1) Discovery.** For each task phase and obstacle, we enumerate candidate spatial predicates (e.g., RightOf, Above) combined with temporal operators (G_I, F_I) bounded to the phase interval I . A candidate φ_k is retained only if it is satisfied by every demonstration, i.e. its worst-case robustness across \mathcal{D} is positive. We keep the two most robust candidates per phase–obstacle pair and conjoin them into a compound specification $\Phi = \bigwedge_k \varphi_k$. **(2) Margin optimization.** Each selected predicate φ_k is augmented with a learnable margin $\epsilon_k \geq 0$. We maximise the total margin while ensuring all demonstrations remain satisfied:

$$\max_{\{\epsilon_k\}} \sum_k \epsilon_k \text{ s.t. } \min_{\xi \in \mathcal{D}} \left[\min_k (\tilde{\rho}(\xi, \varphi_k, 0) - \epsilon_k) \right] \geq 0. \quad (15)$$

The learned ϵ_k values represent the tightest safety margins that all demonstrations respect. Table II summarizes the discovered specification that characterizes the spatial orientation of the arm trajectories relative to each obstacle.

C. Task III: Geometric Accuracy Analysis

A frequent concern for smooth relaxations is whether they preserve geometric meaning. We therefore quantify numeric agreement between our differentiable predicates and a classical geometry engine on randomized convex polygon pairs under random translations/rotations. We evaluate: (i)

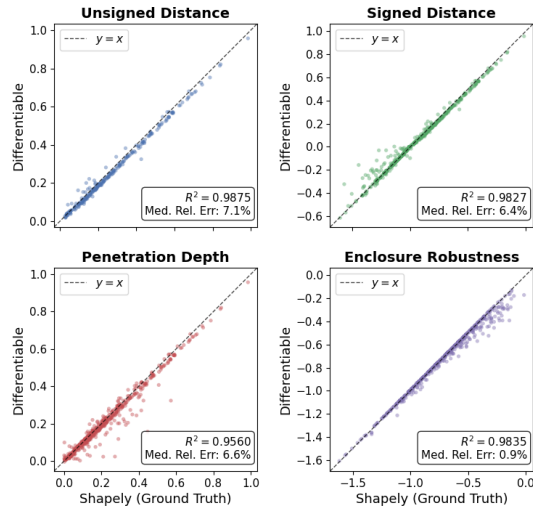


Fig. 8: Geometric accuracy of differentiable predicates. We compare distance, signed distance, penetration, and enclosure robustness against Shapely across randomized convex polygons and transforms.

unsigned distance, (ii) signed distance / penetration depth, and (iii) containment robustness. We report relative errors and summarize distributions in Fig. 8. In practice, increasing boundary samples and decreasing τ improves fidelity at the cost of reduced gradient smoothness.

VI. CONCLUSION

In this paper, we presented *Differentiable SpaTiaL*, a novel framework that bridges formal SpaTiaL and gradient-based robotic optimization. By formulating smooth, tensorized approximations of geometric predicates such as SAT-based penetration and boundary-sampled distance, we established an unbroken gradient flow from high-level semantics to physical states. Our results demonstrate that this architecture enables efficient trajectory synthesis and specification learning in complex, cluttered environments. Future work will extend these differentiable semantics to 3D mesh representations and investigate their integration with deep reinforcement learning policies.

REFERENCES

- [1] O. Maler and D. Nickovic, "Monitoring temporal properties of continuous signals," in *International symposium on formal techniques in real-time and fault-tolerant systems*. Springer, 2004, pp. 152–166.
- [2] G. E. Fainekos and G. J. Pappas, "Robustness of temporal logic specifications for continuous-time signals," *Theoretical Computer Science*, vol. 410, no. 42, pp. 4262–4291, 2009.
- [3] A. Donzé and O. Maler, "Robust satisfaction of temporal logic over real-valued signals," in *Formal Modeling and Analysis of Timed Systems (FORMATS)*, ser. Lecture Notes in Computer Science, vol. 6246. Springer, 2010, pp. 92–106.
- [4] C. Pek, G. F. Schuppe, F. Esposito, J. Tumova, and D. Kragic, "Spatial: monitoring and planning of robotic tasks using spatio-temporal logic specifications," *Autonomous Robots*, 2023.
- [5] C. Belta, B. Yordanov, and E. A. Gol, *Formal Methods for Discrete-Time Dynamical Systems*. Springer, 2017.
- [6] S. M. LaValle, *Planning Algorithms*. Cambridge University Press, 2006.

- [7] N. Ratliff, M. Zucker *et al.*, "Chomp: Gradient optimization techniques for efficient motion planning," in *IEEE International Conference on Robotics and Automation (ICRA)*. IEEE, 2009.
- [8] M. Zucker *et al.*, "Chomp: Covariant hamiltonian optimization for motion planning," *IJRR*, 2013.
- [9] M. Kalakrishnan and S. o. Chitta, "Stomp: Stochastic trajectory optimization for motion planning," in *IEEE International Conference on Robotics and Automation (ICRA)*. IEEE, 2011.
- [10] J. Schulman, J. Ho, C. Lee, I. Awwal, H. Bradlow, and P. Abbeel, "Motion planning with sequential convex optimization and convex collision checking," *The International Journal of Robotics Research*, vol. 33, no. 9, pp. 1251–1270, 2014.
- [11] M. Mukadam, J. Dong *et al.*, "Continuous-time gaussian process motion planning via probabilistic inference," *The International Journal of Robotics Research*, 2018.
- [12] K. Leung, N. Aréchiga, and M. Pavone, "Backpropagation through signal temporal logic specifications: Infusing logical structure into gradient-based methods," 2021.
- [13] P. Kapoor, K. Mizuta, E. Kang, and K. Leung, "Stlpg++: A masking approach for differentiable signal temporal logic specification," *IEEE Robotics and Automation Letters*, 2025.
- [14] S. Gillies and T. S. Developers, *Shapely User Manual*, Shapely Project, 2025, accessed: 2026-03-02.
- [15] J. Pan, S. Chitta, and D. Manocha, "Fcl: A general purpose library for collision and proximity queries," in *International Conference on Robotics and Automation (ICRA)*. IEEE, 2012, pp. 3859–3866.
- [16] E. G. Gilbert, D. W. Johnson, and S. S. Keerthi, "A fast procedure for computing the distance between complex objects in three-dimensional space," *IEEE Journal on Robotics and Automation*, 1988.
- [17] C. Ericson, *Real-Time Collision Detection*. CRC Press, 2004.
- [18] F. de Avila Belbute-Peres, K. Smith *et al.*, "End-to-end differentiable physics for learning and control," in *Advances in Neural Information Processing Systems (NeurIPS)*, 2018.
- [19] J. Degraeve, M. Hermans *et al.*, "A differentiable physics engine for deep learning in robotics," *Frontiers in Neurorobotics*, 2019.
- [20] Y. Hu, L. Anderson *et al.*, "DiffTaichi: Differentiable programming for physical simulation," in *International Conference on Learning Representations (ICLR)*, 2020.
- [21] L. Montaut, Q. Le Lidec *et al.*, "Differentiable collision detection: A randomized smoothing approach," in *IEEE International Conference on Robotics and Automation (ICRA)*. IEEE, 2023.
- [22] Q. Le Lidec, L. Montaut, Y. de Mont-Marin, and J. Carpentier, "End-to-end and highly-efficient differentiable simulation for robotics," *arXiv preprint arXiv:2409.07107*, 2024.
- [23] V. Raman, A. Donzé *et al.*, "Model predictive control with signal temporal logic specifications," in *53rd IEEE Conference on Decision and Control*. IEEE, 2014.
- [24] D. Sadigh *et al.*, "Safe control under uncertainty with probabilistic signal temporal logic," in *Robotics: Science and Systems*, 2016.
- [25] Y. V. Pant, H. Abbas, and R. Mangharam, "Smooth operator: Control using the smooth robustness of temporal logic," in *IEEE Conference on Control Technology and Applications (CCTA)*. IEEE, 2017.
- [26] W. Liu, N. Mehdipour, and C. Belta, "Recurrent neural network controllers for signal temporal logic specifications subject to safety constraints," *IEEE Control Systems Letters*, vol. 6, pp. 91–96, 2022.
- [27] S. Jha, A. Tiwari, S. A. Seshia, T. Sahai, and N. Shankar, "Telex: Learning signal temporal logic from positive examples using tightness metric," *Formal Methods in System Design*, 2019.
- [28] A. Puranic, J. Deshmukh, and S. Nikolaidis, "Learning from demonstrations using signal temporal logic," in *Proceedings of the 2020 Conference on Robot Learning*, ser. Proceedings of Machine Learning Research, J. Kober, F. Ramos, and C. Tomlin, Eds. PMLR, 2021.
- [29] M. Vazquez-Chanlatte, S. Jha, A. Tiwari, M. K. Ho, and S. Seshia, "Learning task specifications from demonstrations," in *Advances in Neural Information Processing Systems*, vol. 31, 2018.
- [30] G. Bombara, C.-I. Vasile, F. Penedo, H. Yasuoka, and C. Belta, "A decision tree approach to data classification using signal temporal logic," in *Proceedings of the 19th International Conference on Hybrid Systems: Computation and Control*, 2016, pp. 1–10.
- [31] K. Liang *et al.*, "Learning optimal signal temporal logic decision trees for classification: A max-flow milp formulation," in *IEEE 63rd Conference on Decision and Control (CDC)*. IEEE, 2024.
- [32] D. Li, M. Cai, C.-I. Vasile, and R. Tron, "Learning signal temporal logic through neural network for interpretable classification," in *2023 American Control Conference (ACC)*. IEEE, 2023, pp. 1–6.